Acta Mechanica 125, 169–181 (1997)

ACTA MECHANICA

Nonlinear dynamics of structures assembled by bolted joints

L. Gaul and **J. Lenz,** Stuttgart, Germany

Dedicated to Prof. Dr. Dr. h. c. Franz Ziegler on the occasion of this 60th birthday

(Received April 2, 1997)

Summary. The nonlinear transfer behaviour of an assembled structure such as a large lightweight space structure is caused by the nonlinear influence of structural connections. Bolted or riveted joints are the primary source of damping compared to material damping, if no special damping treatment is added to the structure. Simulation of this damping amount is very important in the design phase of a structure. Several well known lumped parameter joint models used in the past to describe the dynamic transfer behaviour of isolated joints by Coulomb friction elements are capable of describing global states of slip and stick only.

The present paper investigates the influence of joints by a mixed experimental and numerical strategy. A detailed Finite Element model is established to provide understanding of different slip-stick mechanisms in the contact area. An advanced lumped parameter model is developed and identified by experimental investigations for an isolated bolted joint. This model is implemented in a Finite Element program for calculating the dynamic response of assembled structures incorporating the influence of micro- and macroslip of several bolted joints.

List of symbols

a	acceleration
E_0, E_t	material moduli
F_0	mass weighted excitation force
F_t	tangential joint force
F	generalized force
F^*_{exc}	excitation force
F_{exc}	amplitude of excitation force
F_{C0}	spring element force
F_{R0}	friction element force
K_A, K_B	normal stiffness
K_t	tangential stiffness
L	length of contact area
M_t	transmitted joint torque
m_{red}	reduced mass
p	normal contact pressure
r	effective radius
q	generalized coordinate
z	internal variable
x	coordinate in the contact area
Δu	relative displacement
$\Delta \dot{u}$	relative velocity
$\Delta \varphi$	relative angle

μ friction coefficient
ϑ damping ratio
λ material parameter
σ_0 equivalent slip limit
$\varkappa$ microslip parameter
Ω excitation frequency

1 Introduction

Proper design of a dynamically loaded structure has to take the nonlinear transfer behaviour of joints into account in order to avoid significant deviations between model simulations and real structural response. The influence of joints on structural dynamics depends on the individual joint design. E.g. bolted lap joints cause local stiffness and damping changes when connecting rod or beam structures. This is why the existence of joints leads to small changes of resonance frequencies and the reduction of vibration amplitudes associated with the nonlinear effects. The increase of equivalent damping due to joints is significant in structures with small material damping [2], if no additional damping treatment is added to a structure. The actual normal contact pressure distribution in a dynamically loaded lap joint is not uniform in the interface [3]. Depending on the transmitted load, the contact interface is divided into stick and slip zones. Before gross slip behaviour occurs, the so called macroslip, only local slip exists, the so called microslip [5]. The present paper investigates the influence of joints on the dynamic behaviour by a mixed experimental and numerical strategy. The first step is to measure the dynamic behaviour of an isolated joint. The joint is implemented into a two mass resonator to avoid the influence of connected structures. Different degrees of freedom were analyzed. A detailed Finite Element model of the isolated bolted lap-joint is established to provide deeper insight into the physics of the contact area and allows proper interpretation of the measured results. Then an advanced lumped parameter model is developed and implemented as a nonlinear substructure modul into a Finite Element program. Finally the response of a space structure such as a satellite mast with several bolted joints is calculated. A comparison with an equivalent linear model shows the significance of the nonlinear influence of the connections.

2 Experimental investigation of isolated joints

By implementing the lap joint between two lumped masses with an additional flexure spring so that the system is a resonator, the isolation of the joint is achieved and different modes of joint deformation can be analyzed separately. Longitudinal and torsional vibrations are excited and measured at resonance.

2.1 Longitudinal resonator

The two parts of the resonator are bolted together at the lap joint and suspended by flexible nylon cords at each center of gravity. The attachment location of the shaker is shown in Fig. 2. A flexible connecting rod placed between the excitation point at the force pickup and the shaker assures shear force free excitation. The joint normal pressure is measured by a strain gauge mounted on the joint bolt. The accelerations $a_1(t)$ and $a_2(t)$, and the driving force are measured by piezoelectric pickups. The tangential force F_t is equivalent to the product of the acceleration $a_2(t)$ and the mass of the right part of the resonator. For the force-diplacement hysteresis loops, a double

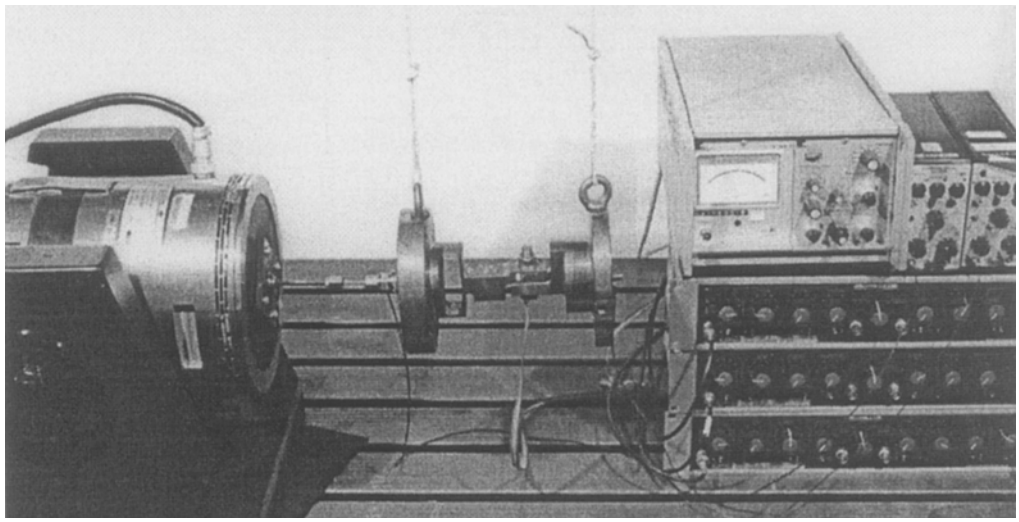

Fig. 1. Experimental setup with longitudinal resonator and isolated lap joint

integration of the acceleration signals is necessary to obtain displacements. Because of superimposed noise in the measured signals, the integration by the amplifier does not lead to sufficient results. Time averaging of the signals [2] smoothens the results but creates small systematic errors in the displacements signals. The chosen procedure here is to cut off the low frequency noise after transformation into the frequency domain by FFT. The remaining signals are integrated twice in frequency domain, leading subsequently to the signals in time domain by inverse Fourier transformation. The measured hysteresis loops in Fig. 3 correspond to an excitation frequency of 460 Hz and a joint interface pressure of $p = 0.25$ N/mm^2. The hysteresis curves in Fig. 3 are plotted for a measuring time of 0.5 s which is equivalent to 233 vibration periods. Without additional time averaging each hysteresis shows only negligible noise. For large excitation forces,

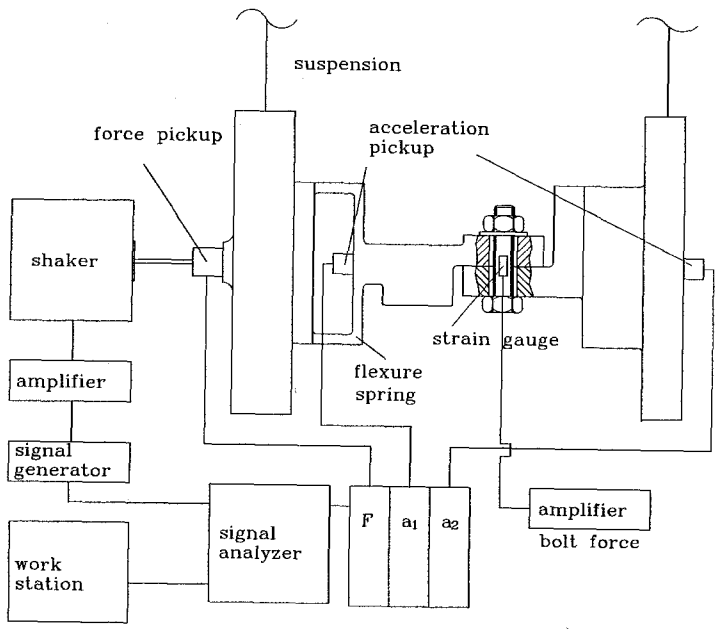

Fig. 2. Measuring equipment of the longitudinal resonator

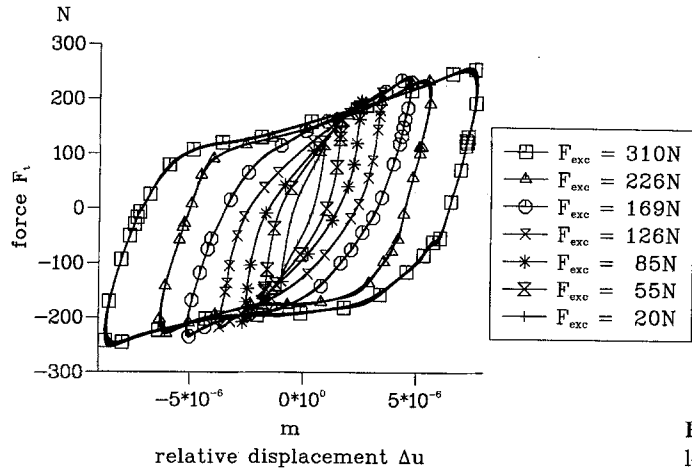

Fig. 3. Measured hysteresis of the longitudinal resonator

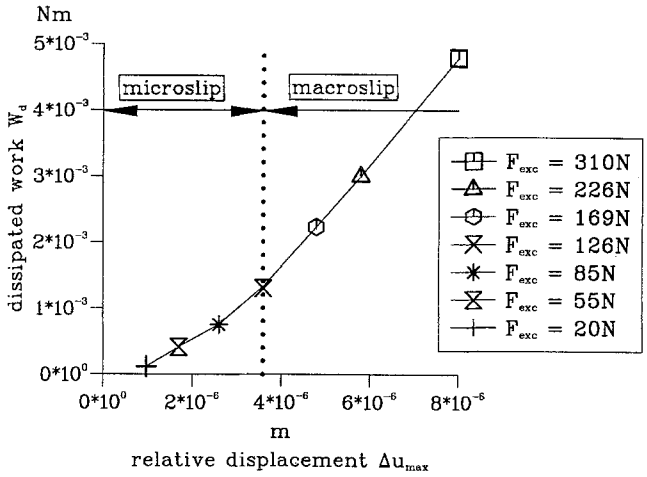

Fig. 4. Measured dissipated work of the longitudinal resonator

slip and stick behaviour can be well distinguished by the two different slopes. In the range of excitation force F_{exc} between 85 N and 169 N, the transition from microslip to macroslip takes place. Excitation forces below the lower limit lead to sharp corners of the hysteresis when the relative velocity changes sign. In the transition range between micro- and macroslip, the hysteresis is rounded at the corners. It can be noticed as well that macroslip leads to a slight increase of the transmitted force with growing relative displacement. Important conclusions can be drawn from the energy dissipation per vibration cycle. The area of the closed hysteresis loop for periodic signals representing dissipated work is plotted in Fig. 4 versus the amplitude of the relative displacement. The nearly straight line portion represents gross slip behaviour in the range of large excitation forces. In the range of smaller excitation forces between 20 N and 126 N, the dissipated work shows an increasing slope with increasing relative displacement.

2.2 Torsional resonator

Frequently, bolted connections have to transmit bending moments as well as normal forces and shear forces. Torques are transmitted in bolted flange connections.

To isolate the transmission of such moments, a torsional resonator was designed with an isolated bolted joint (Fig. 5). The resonator is suspended by a nylon cord fixed at the top in the

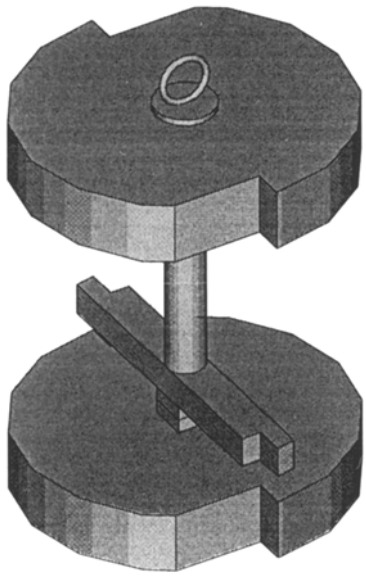

Fig. 5. Resonator with torsional excitation

direction of the rotation axis as shown in Fig. 6. The joint normal pressure is controlled by a compressed helical spring. The measuring and data processing equipment for the longitudinal resonator in Fig. 2 was used for the torsional resonator as well. The shaft of the torsional resonator serves as torsional spring like the flexure spring used in the longitudinal resonator (Fig. 6). Figure 7 shows measured hysteresis curves corresponding to 6 different excitation force amplitudes. The forces are applied by a shaker via a connecting rod at the outer radius of the upper resonator mass.

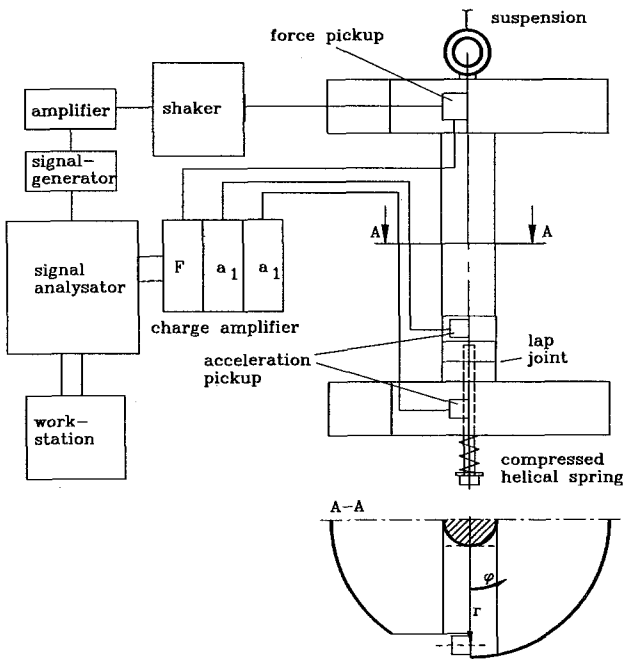

Fig. 6. Measurement equipment of the torsional resonator

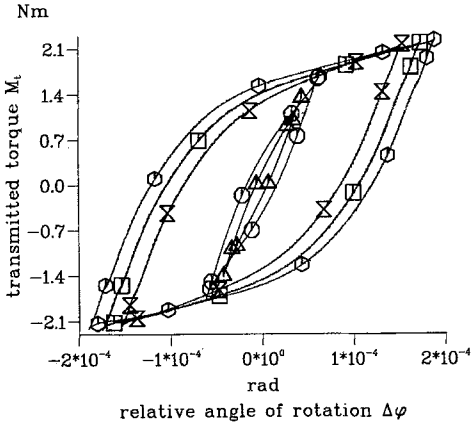

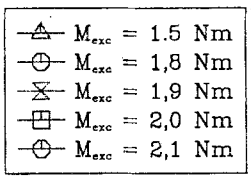

Fig. 7. Measured hysteresis of the torsional resonator

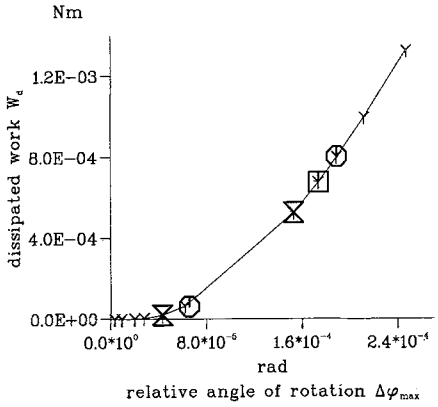

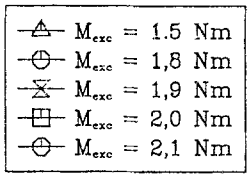

Fig. 8. Measured dissipated work of the torsional resonator

The excitation frequency was 87 Hz and the joint pressure $p = 1$ N/mm^2. The hysteresis shapes shown in Fig. 7 are quite similar to those of the joint with longitudinal force excitation. Macroslip is identified above a torque corresponding to the excitation force amplitude $F_{exc} = 22$ N by visible relative displacements between the boundaries of the contacting interfaces. Figure 8 depicts the dissipated work per cycle versus the amplitudes of the angle of relative rotation. The two ranges are separable by the straight line segment in the macroslip range and the curve segment with variable slope in the microslip range. Additional measurements marked by Y in Fig. 8, underline these ranges.

3 Finite Element analysis of longitudinal resonator

To gain more information about the mechanisms at different contact states, a two dimensional Finite Element model of the longitudinal resonator is analyzed. The resonator is discretized with four node plane stress elements (Fig. 9). The following assumptions are made: the longitudinal resonator masses are lumped, the flexure spring is replaced by a longitudinal spring, the bolt hole and the bolt shaft are neglected and the pressure distribution in the contact area is due to uniformly distributed normal force applied as static preload at the top and the bottom of the lap joint (Fig. 10). After the normal forces are applied, the model is subjected to a tangential force equivalent to the driving force of the experimental resonator.

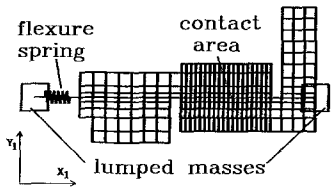

Fig. 9. FE-model of the resonator

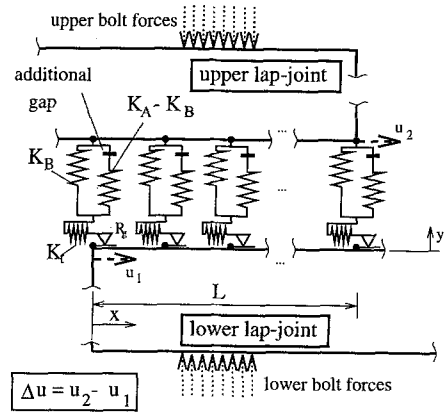

Fig. 10. Contact model of lap joint

In the contact area of the model, gap friction elements (Fig. 10) with Coulomb type constitutive equation represent the frictional interface. Furthermore, it is possible to use additional springs in both directions of the plane model to simulate an intermediate layer. Due to the static preload, the additional gaps are closed during the whole calculation. Along the contact area, the coordinate x is introduced and normalized by the entire length L. In a first investigation, the normal gap stiffness K_A is varied. In case of a small stiffness $K_A = 10000$ N/mm (Fig. 11), uniform distribution of the pressure appears along the contact area. For larger stiffness $K_A = 100000$ N/mm, the pressure increases from both ends to a maximum level at the middle of the contact area (x/L = 0.5). The Coulomb slip limit is proportional to the normal pressure with friction coefficient μ which varies along the contact area. For a constant distribution of the slip limit along the whole contact area ($K_A = 10000$ N/mm) all coulomb elements exceed their slip limits at the same time. In this case there is a change between stick and global slip without any transition between the different slopes (Fig. 12). For $K_A = 100000$ N/mm the contact areas at both ends begin to slide first, while in the middle of the contact area (x/L = 0.5) no slip occurs

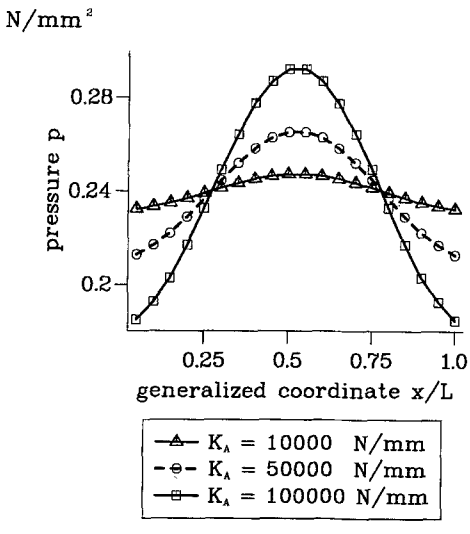

Fig. 11. Distribution of contact pressure

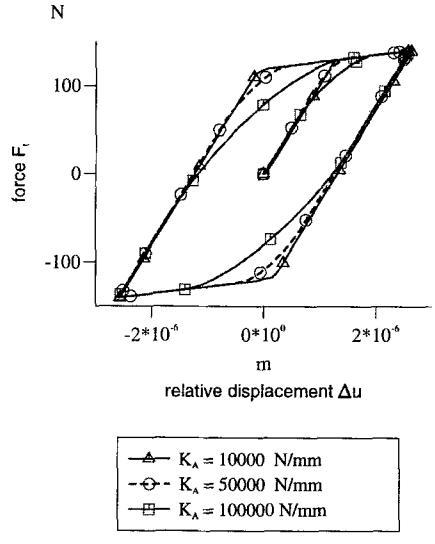

Fig. 12. Calculated hysteresis

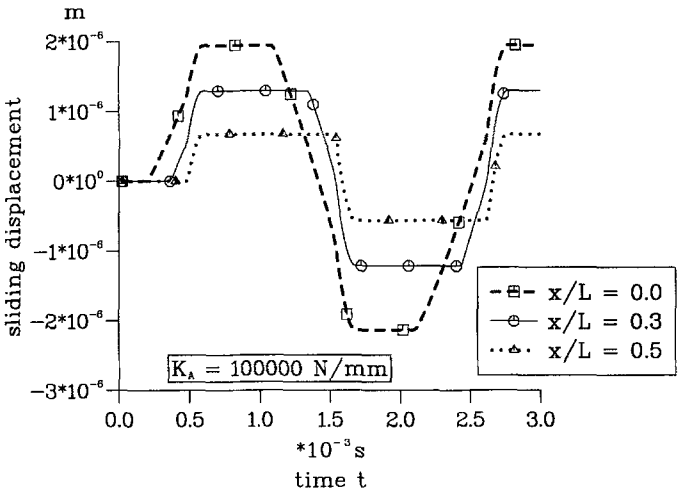

Fig. 13. Sliding displacement in gap

(Fig. 13). Then more and more Coulomb elements exceed their slip limits until all elements are in slip state and macroslip occurs. This is the reason why the global hysteresis in Fig. 12 has a rounded transition between the stick and the global macroslip domain. This state, where local stick and slip zones exist simultaneously in the contact area, is called microslip.

Further investigations show, that the elastic displacement of the joint in horizontal direction has negligible influence on the slip behaviour. The influence of the contact surface on a microscale has been studied by statistics in [8].

4 Simulation of microslip and macroslip by the Valanis model

The aim of the study is not only to investigate the dynamic behaviour of single joints, but also of structures assembled by several bolted joints. Therefore, it is important to develop a joint model with only a few parameters. Different joint models which are implemented into a simple two mass resonator have been tested [5].

As only the relative displacement $\Delta u = u_2 - u_1$ between the lumped masses is of interest, the associated equation of motion with periodic excitation force

$$m_{\text{red}} \Delta\ddot{u} = F_t(\Delta u, \Delta\dot{u}) - F_0 \cos(\Omega t), \tag{1}$$

$$m_{\text{red}} = \frac{m_1 m_2}{m_1 + m_2}, \qquad F_0 = \frac{m_1}{m_1 + m_2} F_{\text{exc}} \tag{2}$$

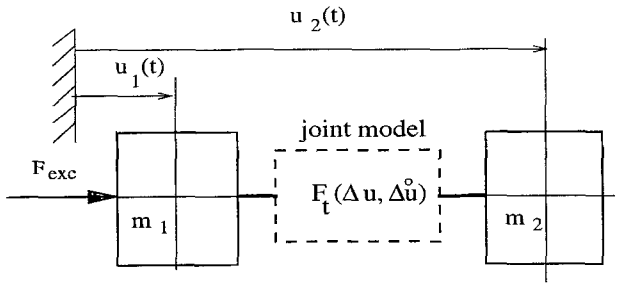

Fig. 14. Two mass resonator with the implemented joint model

represents a SDOF system. To obtain the behaviour of both regimes (micro- and macro-slip) by one model and to simulate response under cyclic loads as well as transient behaviour, the Valanis model known from plasticity [7] has been adopted. Without slip-stick parameters and by assuming velocity independence, the model is governed by the differential equation

$$F'(z) + \lambda F(z) = E_0 q'(z) + \lambda E_t q(z), \tag{3}$$

where F is the generalized force, q is the generalized coordinate, and E_0, E_t and λ are material parameters. In the next steps, the parameters will be identified for the joint description. The relation between the internal variable $z(t)$ and physical time t is given by

$$\dot{z}(t) = \left| \dot{q}(t) - \varkappa \frac{\dot{F}(t)}{E_0} \right|. \tag{4}$$

Differentiation of F and q with respect to z in Eq. (3) is now replaced by

$$F' = \frac{dF}{dz} = \frac{dF}{dt}\frac{dt}{dz}, \qquad q' = \frac{dq}{dz} = \frac{dq}{dt}\frac{dt}{dz}. \tag{5}$$

Insertion of Eq. (5) in Eq. (3) leads to

$$\dot{F}\frac{1}{\dot{z}} + \lambda F = E_0 \dot{q}\frac{1}{\dot{z}} + \lambda E_t q, \tag{6}$$

and replacement of $\dot{z}$ using Eq. (4) yields

$$\dot{F} = E_0 \dot{q} + \lambda \left| \dot{q} - \varkappa \frac{\dot{F}}{E_0} \right| (E_t q - F). \tag{7}$$

By restricting the parameter $\varkappa$:

$$0 \leqq \varkappa < 1, \tag{8}$$

an equivalent formulation in the following expression is possible

$$\left| \dot{q} - \varkappa \frac{\dot{F}}{E_0} \right| = \frac{\dot{q}}{|\dot{q}|}\left(\dot{q} - \varkappa \frac{\dot{F}}{E_0} \right). \tag{9}$$

Insertion of Eq. (9) in Eq. (7) leads to the evolution equation of the joint hysteresis as differential equation of first order

$$\dot{F} = \frac{E_0 \dot{q}\left[1 + \dfrac{\lambda}{E_0}\dfrac{\dot{q}}{|\dot{q}|}(E_t q - F) \right]}{1 + \varkappa \dfrac{\lambda}{E_0}\dfrac{\dot{q}}{|\dot{q}|}(E_t q - F)} = f(q, \dot{q}, F). \tag{10}$$

If we interprete

$$q = \Delta u \qquad F = F_t \tag{11}$$

it is possible to couple Eq. (10) for the joint model with the equation of motion Eq. (1) of the resonator. This leads to the following differential equation in terms of the relative displacement Δu

$$m_{\mathrm{red}} \Delta \ddot{u} = \frac{\mathrm{E}_0 \Delta \dot{u}\left[1 + \dfrac{\lambda}{E_0}\dfrac{\Delta \dot{u}}{|\Delta \dot{u}|}(E_t \Delta u - F) \right]}{1 + \varkappa \dfrac{\lambda}{E_0}\dfrac{\Delta \dot{u}}{|\Delta \dot{u}|}(E_t \Delta u - F)} + F_0 \Omega \sin(\Omega t). \tag{12}$$

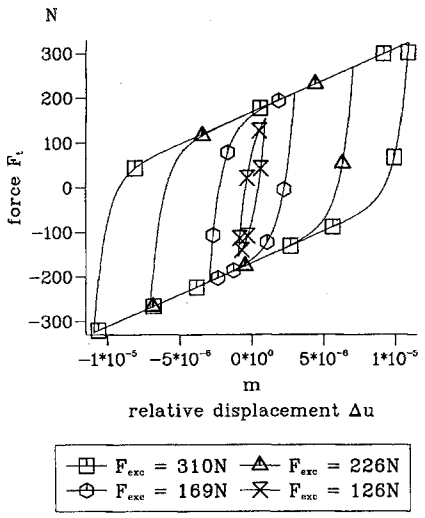

Fig. 15. Macroslip hysteresis

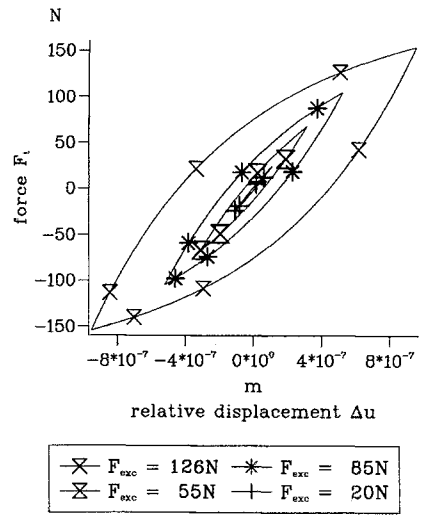

Fig. 16. Microslip hysteresis

The stiffness modul of the stick condition is denoted by E_0 while the tangent modulus E_t describes the slope of slip motion. The parameter $\varkappa$ controls the influence of microslip. High values of $\varkappa$ correspond to small influence of microslip. The parameter σ_0 denotes a stick limit equivalent to the yield stress as being defined in [4]:

$$\sigma_0 = \frac{E_0}{\lambda\left(1 - \varkappa \frac{E_t}{E_0}\right)}. \tag{13}$$

The parameters of the joint model in Eq. (10) are identified from a single measured hysteresis and by an iterative fit of $\varkappa$. Figures 15 and 16 show hysteresis curves for 7 different excitation force amplitudes. They were extrapolated from the hysteresis model with parameters identified for the low normal pressure of $p = 0.25$ N/mm^2 and the excitation force amplitude of $F_{exc} = 310$ N as shown in Fig. 3

$E_0 = 2.2 * 10^8$ N/mm^2 $\quad E_t = 1.4 * 10^7$ N/mm^2

$\sigma_0 = 180$ N $\quad \varkappa = 0.01$

5 Implementation of the Valanis model as a nonlinear substructure modul into finite element software

Equation (10) of the Valanis model is implemented as user defined modul into the Finite Element Software MARC [6]. It is possible to simulate the dynamic response of a structure assembled with bolted joints. In an example, the dynamic response of an assembled structure such as the spaceframe mast shown in Fig. 17 is calculated. A selected simplified 2-D FE-model in Fig. 18 consists of 133 beam elements, one additional tip mass and 15 Valanis elements. The Valanis elements connect the rotational degrees of freedom at each pin joint. The parameters of the Valanis model are identified from the measured hysteresis of the isolated torsional resonator

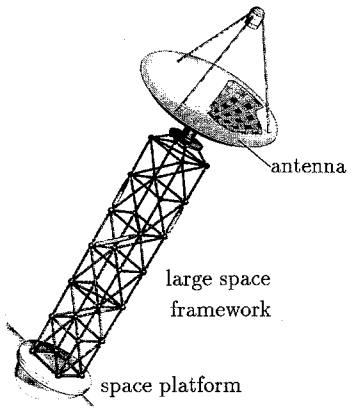

Fig. 17. Space structure [1]

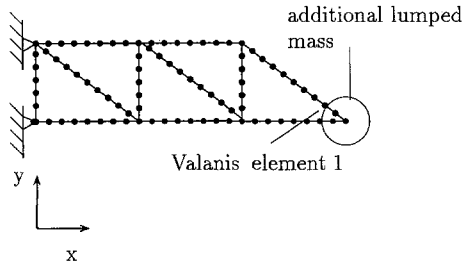

Fig. 18. Twodimensional beam FE model

(Fig. 7). In this example the damping of the longitudinal motion is neglected. The FE-model of the space structure is excited with a force impulse near the additional tip mass in vertical direction. The structure is fixed at two nodes on the left side (Fig. 18).

The response is compared with the response of an equivalent linear FE-model with a material damping ratio of $\vartheta = 0.1\%$ only. Figure 19 shows the damped response. The displacement amplitude of the structure including the Valanis model decreases faster when compared to the curve with material damping only.

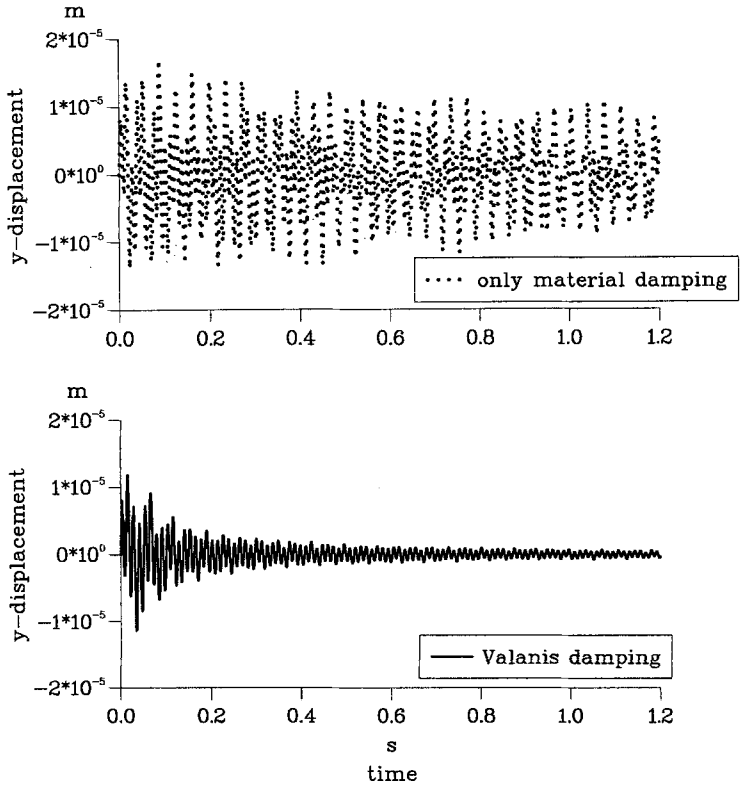

Fig. 19. Vertical-displacement of the tip mass (— Valanis damping included)

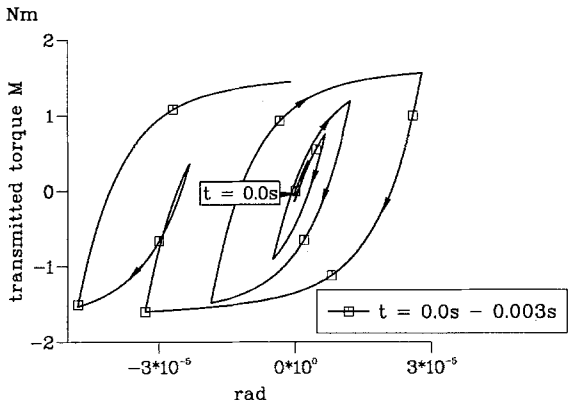

Fig. 20. Valanis element 1 after $t = 0$ s

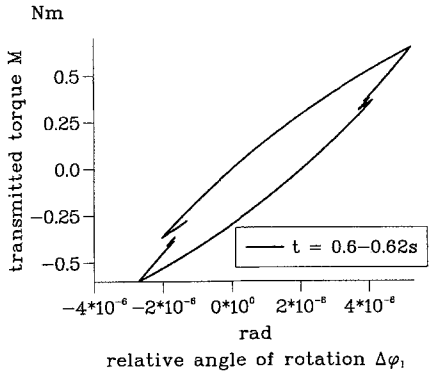

Fig. 21. Valanis element 1 after 0.6 s

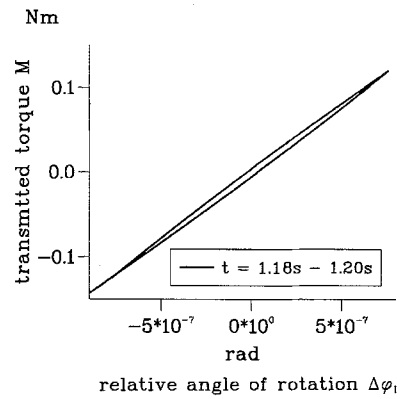

Fig. 22. Valanis element 1 after 1.18 s

Figures 20–22 show the hystereses of the Valanis element 1 between the two beams at the additional tip mass for different times. When the oscillation starts, the slip limit of the Valanis element is exceeded and macroslip occurs (Fig. 20).

Because of high damping, the amplitude of the relative angle of rotation decreases and a typical microslip hysteresis appears after 0.6 s. The slip limit is no longer reached, but energy is still dissipated (Fig. 21). Figure 22 shows the hysteresis shape after 1.18 s. There is only little damping left, but the damping of all Valanis elements is still larger than the material damping of the linear model.

6 Conclusion

The dynamics of assembled structures is influenced by the nonlinear transfer behaviour of its connections. Bolted and riveted joints are the primary source of damping. Therefore it is desirable to predict the dynamic response of an assembled structure in the design phase. The present paper investigates the dynamic transfer behaviour of bolted joints with a mixed experimental and numerical strategy. The transfer behaviour of an isolated joint is measured first for different modes of vibration and than analyzed by using a detailed FE-model. To improve the ability of lumped Coulomb models restricted to stick and macroslip description only, the Valanis

model known from plasticity is adopted, tested and implemented in a FE-software package for simulating micro- as well as macroslip in joints of assembled structures. As an example, the calculated 2-D response of a space structure model demonstrates the nonlinear influence of the connections by the rapid decay of free vibrations of the assembled structure. With this FE-modul it is possible to predict the response of assembled structures in the design phase or to predict the influence of structural modifications, if sufficient knowledge of the behaviour of the individual joints is available.

References

[1] Breitbach, E. J., Lammering, R., Melcher, J.: Nitzsche, F.: Smart structures research in aerospace engineering. Proc. of Second European Conference on Smart Structures and Materials, Glasgow, U. K., pp. 11–18, 1994.

[2] Gaul, L., Bohlen, S.: Identification of nonlinear structural joint models and implementation in discretized structure models. Proc. 11th ASME Conference on Mechanical Vibration and Noise: The Role of Damping in Vibration and Noise, Boston (USA), **5,** 213–219 (1987).

[3] Gaul, L., Nackenhorst, U., Willner, K., Lenz, J.: Nonlinear vibration damping of structures with bolted joints. Proc. of IMAC XII, Honolulu **12,** pp. 875–881 (1994).

[4] Haupt, P.: Dynamische Systeme mit geschwindigkeitsunabhängiger Dämpfung. ZAMM **71,** T 55–T 57 (1991).

[5] Lenz, J., Gaul, L.: The influence of microslip to the dynamic behaviour of bolted joints. Proc. of IMAC XIII, Nashville **13,** pp. 248–254 (1995).

[6] MARC Analysis Research Corporation, Palo Alto. MARC Programm Documentation, 1990.

[7] Valanis, K. C.: Fundamental consequences of a new intrinsic time measure. Plasticity as a limit of the endochronic theory. Arch. Mech. **32,** 171–191 (1980).

[8] Willner, K., Gaul, L.: A penalty approach for contact description by FEM based on interface physics. Contact Mechanics II, Computational Mechanics Publications Southampton (Aliabadi, Alessandri, eds.), pp. 257–264, 1995.

Authors' address: Prof. Dr.-Ing. L. Gaul and Dr.-Ing. J. Lenz, Institut A für Mechanik, Universität Stuttgart, D-70550 Stuttgart, Germany